

Integration of Graphene Electrodes with 3D Skeletal Muscle Tissue Models

Yongdeok Kim, Gelson Pagan-Diaz, Lauren Gapinske, Yerim Kim, Judy Suh, Emilia Solomon, Jennifer Foster Harris, SungWoo Nam, and Rashid Bashir*

Integration of conductive electrodes with 3D tissue models can have great potential for applications in bioelectronics, drug screening, and implantable devices. As conventional electrodes cannot be easily integrated on 3D, polymeric, and biocompatible substrates, alternatives are highly desirable. Graphene offers significant advantages over conventional electrodes due to its mechanical flexibility and robustness, biocompatibility, and electrical properties. However, the transfer of chemical vapor deposition graphene onto millimeter scale 3D structures is challenging using conventional wet graphene transfer methods with a rigid poly (methyl methacrylate) (PMMA) supportive layer. Here, a biocompatible 3D graphene transfer method onto 3D printed structure using a soft poly ethylene glycol diacrylate (PEGDA) supportive layer to integrate the graphene layer with a 3D engineered ring of skeletal muscle tissue is reported. The use of softer PEGDA supportive layer, with a 10^5 times lower Young's modulus compared to PMMA, results in conformal integration of the graphene with 3D printed pillars and allows electrical stimulation and actuation of the muscle ring with various applied voltages and frequencies. The graphene integration method can be applied to many 3D tissue models and be used as a platform for electrical interfaces to 3D biological tissue system.

engineering because of its unique optical, electrical, mechanical, and biological characteristics.^[1–3] Graphene and its derivatives have also found many applications in tissue engineering and regenerative medicine.^[4,5] Among its tissue engineering applications, the enhanced adhesion, proliferation, and myogenesis of skeletal muscle cells on graphene have been reported on 2D substrates.^[6–8] Although 3D structured graphene systems have been reported as a tissue scaffold using 3D printing or dry spinning with graphene derivatives, such as reduced graphene oxide or graphene oxide, they have a limited electrical conductivity due to the presence of an insulating additive polymer and/or defect functional groups.^[2,9–12] Chemical vapor deposition (CVD) synthesized graphene, on the other hand, is known to be more uniform and compatible with large area synthesis.^[13,14]

Previous works have been reported on 3D integration using CVD grown graphene.^[15–18] Lanza et al. and Shim et al.

Graphene, a 2D monolayer of sp^2 -bonded carbon with honeycomb lattice structure, is a promising nanomaterial for applications, such as bioelectronics, imaging, drug delivery, and tissue

integrated graphene onto pyramidal atomic force microscopy tips with a thin poly (methyl methacrylate) (PMMA) film as a supportive layer.^[15,16] Choi et al. used a 3D patterned swollen

Y. Kim
Department of Materials Science and Engineering
and Nick J. Holonyak Micro and Nanotechnology Laboratory
University of Illinois Urbana-Champaign
Urbana, IL 61801, USA

G. Pagan-Diaz, L. Gapinske
Department of Bioengineering and Nick J. Holonyak Micro
and Nanotechnology Laboratory
University of Illinois Urbana-Champaign
Urbana, IL 61801, USA


Y. Kim
Department of Mechanical Science and Engineering
University of Illinois Urbana-Champaign
Urbana, IL 61801, USA

J. Suh
Department of Chemistry
University of Illinois Urbana-Champaign
Urbana, IL 61801, USA

Dr. E. Solomon, Dr. J. F. Harris
Bioscience Division
Los Alamos National Laboratory
Los Alamos, NM 87545, USA

Prof. S. W. Nam
Department of Mechanical Science and Engineering and Department
of Materials Science and Engineering
University of Illinois Urbana-Champaign
Urbana, IL 61801, USA

Prof. R. Bashir
Department of Bioengineering
Nick J. Holonyak Micro and Nanotechnology Laboratory
and Carle Illinois College of Medicine
University of Illinois Urbana-Champaign
Urbana, IL 61801, USA
E-mail: rbashir@illinois.edu

 The ORCID identification number(s) for the author(s) of this article can be found under <https://doi.org/10.1002/adhm.201901137>.

DOI: 10.1002/adhm.201901137

polydimethylsiloxane (PDMS) to transfer PMMA coated graphene onto various 3D features, such as pyramids, domes, and pillars ranging from 3.5 to 50 μm .^[17] They used a thinner PMMA as a supportive layer for 3D graphene transfer to reduce flexural rigidity. However, the rigid PMMA is still limited for 3D integration with other polymeric substrates or at larger scales. Other than PMMA, Morin et al. used PDMS and polyimide film as a supportive layer and applied vacuum to result in conformal integration of graphene onto the 3D printed implant.^[18] However, this platform had variable coverage of graphene ranging from 74% to 95% and no electrical application of 3D graphene was demonstrated. Realizing electrical contacts to 3D tissue models can result in new ways to interrogate the function of these biological tissues.

Skeletal muscles, serving the primary actuator in animals, have also been used as biohybrid actuators in soft robotics.^[19–21] Integration of 3D engineered skeletal muscle embedded in extracellular matrix on 3D printed hydrogel skeleton have been shown for walking or pumping functions using electrical or optical stimulation.^[22–24] If these biohybrid machines can be integrated with electronics, a suite of applications can be possible for electrical actuation control and sensing.

Here, we report a biocompatible 3D graphene transfer method using a PEGDA supportive layer and its integration with a 3D skeletal muscle ring. A softer PEGDA layer enabled the conformal integration of graphene with a millimeter-scale 3D printed PEGDA pillars. Considering that PEG is an Food and Drug Administration approved biocompatible material, it is well suited to 3D biological application with integrated electronics. As an electrical application of our 3D electrode integrated tissue system, a 3D skeletal muscle ring on the integrated structure was actuated electrically with different voltages and frequencies via the transferred graphene contacts to muscle ring. This platform can provide for an electrical contact with 3D in-vitro tissue-on-chip models for drug screening and for applications in the soft robotics.

A PEGDA layer was used as support layer on CVD grown graphene for 3D conformal integration onto millimeter scale 3D printed pillars. The flexural rigidity, defined as the resistance offered by a structure while undergoing bending, is an important factor for 3D integration.^[17] A lower flexural rigidity is beneficial for 3D integration because the film can be more easily deformed under bending. Equation (1) shows that the flexural rigidity is proportional to the Young's modulus, where D is the flexural rigidity, E is the Young's modulus, h is the film thickness, and ν is the Poisson's ratio

$$D = \frac{Eh^3}{12(1-\nu^2)} \quad (1)$$

Hence, a softer PEGDA support layer with a few tens of kPa of E is beneficial for bending than a few GPa range of E for PMMA, which is typically used as graphene support layer. The E is also larger than MPa range of PDMS which Morin et al. used for 3D graphene integration.^[18] Although the spin coated PEGDA layer has thickness of about a micrometer, and is much thicker than usual PMMA coating layer on graphene, the large difference in Young's modulus dominates the lower flexural rigidity of PEGDA layer than that of PMMA. In addition, a

thick PEGDA layer can provide mechanical stability to prevent the graphene layer being torn off during the 3D transfer.

Figure 1 shows the fabrication steps to integrate a graphene sheet on 3D printed pillars and a muscle tissue ring. A PEGDA support layer on CVD grown graphene on copper foil was polymerized by spin coating and UV exposure via the addition of a photoinitiator. The copper foil was etched in ferric chloride based copper etchant after turning PEGDA coated graphene upside down, with graphene layer facing the top and PEGDA at the bottom as shown in Figure 1a. Figure 1b shows the graphene/PEGDA sheet on water after etching of copper. Figure S1 (Supporting Information) shows the microstructure in the scanning electron microscope images of the graphene/PEGDA sheet. Figure 1c–e shows the computer-aided design (CAD) design for printed pillar structure with dimensions to integrate with graphene and muscle, and the side and top images of the structure printed by stereolithography apparatus, respectively. After the graphene/PEGDA sheet was transferred on to printed pillars, the conformal integration of the sheet and pillar structure can be seen in Figure 1f,g. The muscle ring was then prepared with the printed mold shown in Figure 1h. The specific method for creation of the 3D muscle ring is described in Figure S2 (Supporting Information). After the integration of the muscle ring, the graphene/PEGDA sheet is shown in Figure 1i. The detailed fabrication steps and Experimental methods are described in the Supporting Information.

Figure 1j–l shows the graphene characterization after graphene transfer on 3D printed pillars. In Figure 1j, D, G, and 2D bands of graphene's Raman spectra are observed on the top of graphene-transferred pillar structure. Significantly higher 2D band intensity compared to G band implies that the synthesized graphene is a monolayer. Raman shift peaks of PEG are due to the PEGDA supportive layer beneath the graphene. The shifts for 2897 and 2843 cm^{-1} are caused by the symmetric stretching vibration of methylene group in PEG.^[25] Also, the peak for 1470 cm^{-1} of $\text{CH}_2\text{-CH}_2$ bending vibration from PEG is also shown.^[26] The differences in intensity of PEG are similar to other references in that the peaks from symmetric stretching vibration of methylene group is larger than those for $\text{CH}_2\text{-CH}_2$ bending vibration.^[25,26] The Raman measurement clearly shows that the graphene and PEG supportive layer were successfully transferred on the top of pillars.

For many applications, the electrical conductivity of the transferred graphene electrode is an important characteristic. To measure the electrical conductivity of 3D transferred graphene sheet, silver paint was applied on the 4 spots on the graphene sheets shown in Figure 1k. I - V curves were measured by contacting probes on the corresponding painted spots. The difference in resistances between different spots is reasonable because the distance between two points for left and right bottoms is longer than those for other two sets, which they have a similar range of sheet resistance from 77 k to 120 k $\Omega \text{ sq}^{-1}$. Considering around 800 $\Omega \text{ sq}^{-1}$ of graphene sheet resistance and the distance between silver paints, the 3D transferred graphene has a higher resistance than common planar graphene.^[13,27,28] This is because the 3D graphene was supported by a PEGDA hydrogel, which was swollen due to wet transfer and could have resulted in defects in the graphene layer as shown in Figure S3b (Supporting Information, on top of pillar

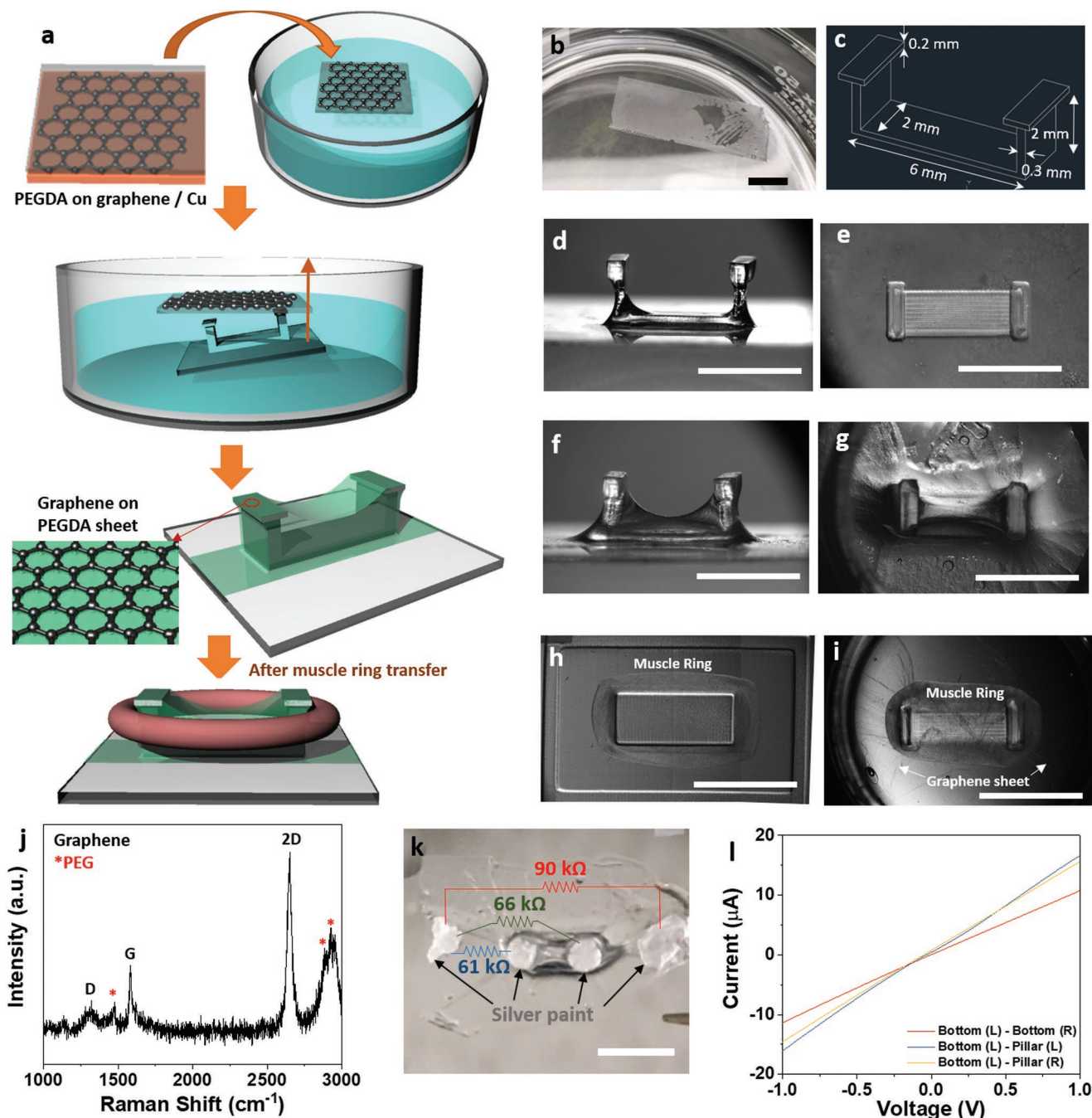


Figure 1. Fabrication for 3D graphene and muscle ring transfer onto the 3D printed PEGDA pillars. a) Schematic to how the integration of the 3D graphene with muscle ring. b) Image of graphene/PEG sheet in DI water after Cu removal. c) 3D CAD image and dimensions of printed PEGDA pillars. d) Side and e) top views of 3D PEG printed pillars. f) Side and g) top views of pillars after graphene transfer. Images for muscle ring h) before transfer in the ring mold and i) on the graphene sheet/PEG pillars after ring transfer. j) Raman signal of graphene/PEG sheet on the top of pillar after graphene transfer. k) The image of silver paints and graphene/PEG sheet on the pillars for measurement of electrical resistance between silver painted electrode. l) I - V curves between left outside and right outside, left outside and on the left pillar, and left outside and on the right pillar. All scale bars are 5 mm.

after 3D transfer). Figure S3a (Supporting Information, same as Figure 1j) indicates that the red spot in Figure S3b (Supporting Information) has Raman peaks for D, G, and 2D bands of graphene and PEG, while the blue circle contains only Raman shifts for PEG and not graphene, as shown in Figure S3c (Supporting Information). Although the 3D transferred graphene

has a higher resistance than planar one, they showed the linear I - V curves and expected Raman shifts.

Figure 2 shows the muscle ring characterization on the 3D graphene integrated with printed pillars. Images of a muscle ring on the structure before ring transfer and on day 1, 3, 5, 7, and 10 after ring transfer are shown. The muscle ring had been formed

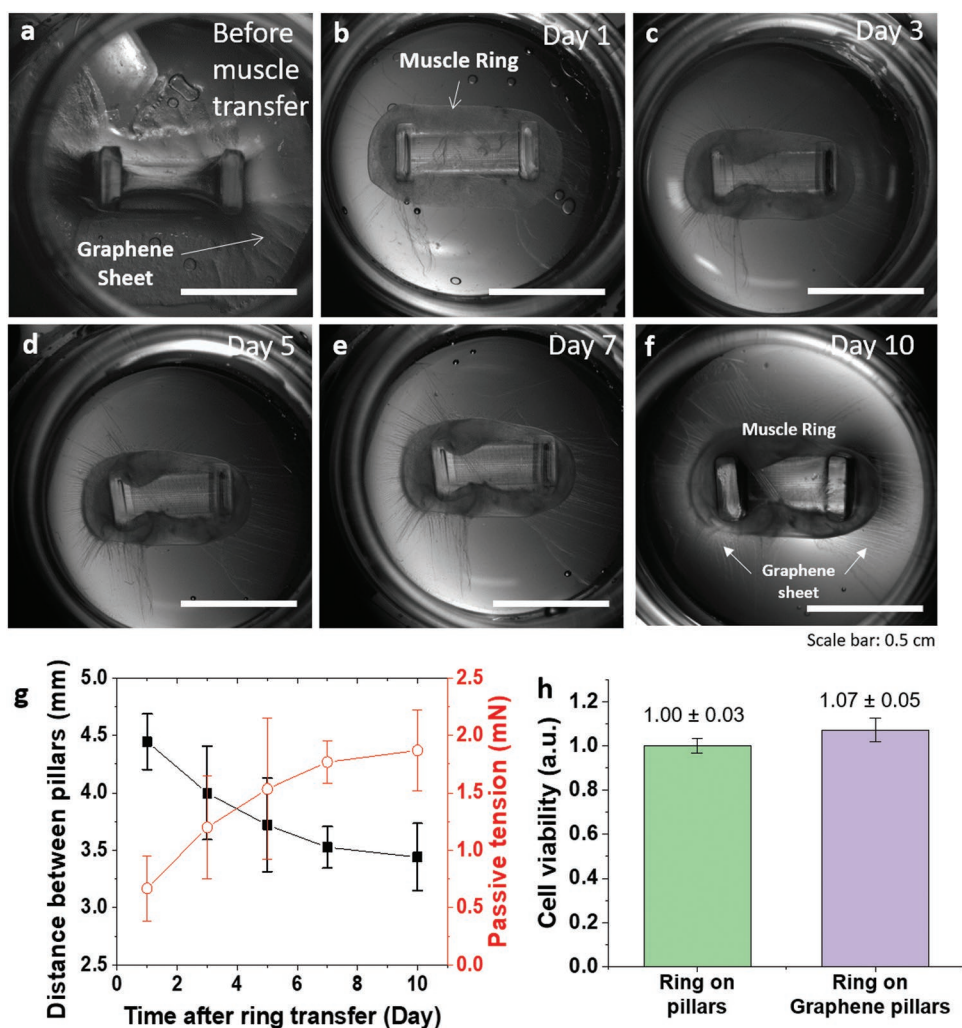


Figure 2. The interaction of muscle ring with 3D graphene/PEG pillars. Optical images of 3D graphene/PEG pillars a) before muscle ring transfer, b) day 1, c) day 3, d) day 5, e) day 7, and f) day 10, after muscle ring transfer. g) The distance between pillars and passive tension with different days after muscle ring transfer ($n = 3$). h) Cell viability as determined by MTS cell proliferation assay of muscle ring on the graphene/PEGDA pillars and PEGDA pillars without graphene on day 5 after ring transfer.

and cultured in differentiation medium for 10 d as described in earlier reports.^[22,23] Graphene sheet 10 d after the ring transfer is shown in Figure 2f. Figure S4 (Supporting Information) shows immunofluorescence images for the aligned longitudinal myotubes in the muscle ring on day 7 after ring transfer on to the 3D graphene integrated structure. As the C2C12 skeletal muscle differentiates from myoblasts to myotubes, the compaction of the muscle ring decreased the distance between the pillars as shown in Figure 2g. The passive tension, calculated based on the Euler–Bernoulli beam-bending theory,^[22] was 0.67 ± 0.28 mN right after the ring transfer and increased to 1.87 ± 0.35 mN on day 10 after ring transfer and is in similar range as previous studies.^[22] The cell viability in the muscle ring was determined by 3-(4,5-dimethylthiazol-2-yl)-5-(3-carboxymethoxyphenyl)-2-(4-sulfophenyl)-2H-tetrazolium (MTS) cell proliferation assays. Cells in muscle rings cultured on graphene sheet showed about 7% higher viability level than those on pillars without the graphene sheet in Figure 2h. This is expected, as graphene is known to promote proliferation and differentiation of the skeletal

muscles.^[6,8] Based on the passive tension results and the cell viability results, it can be concluded that the 3D graphene can be integrated with the tissue in a biocompatible manner.

Next, electrical stimulation was applied to the muscle ring with the transferred graphene electrode, as shown in Figure 3a and Movie S1 (Supporting Information). To make connection with the graphene sheet, silver paint and copper tapes were used for both ends outside the cell culture well as shown in Figure 3b. Figure 3c shows the graphene sheet extended from the muscle ring to the well. When a 5 V signal was applied, no actuation was observed in the pillars. However, increasing the voltage amplitude to 10 and 20 V resulted in a noticeable displacement change as shown in Figure 3e,f, respectively. The average displacements of the pillars were 3.9 ± 1.0 μm for 10 V and 8.2 ± 1.3 μm for 20 V, respectively.

Various pulse frequencies of a given voltage through graphene electrode also resulted in pillar displacement caused by muscle actuation. When a 0.5 Hz, 20 V pulse was applied, the pillars moved with 0.5 Hz as shown Figure 3g. In

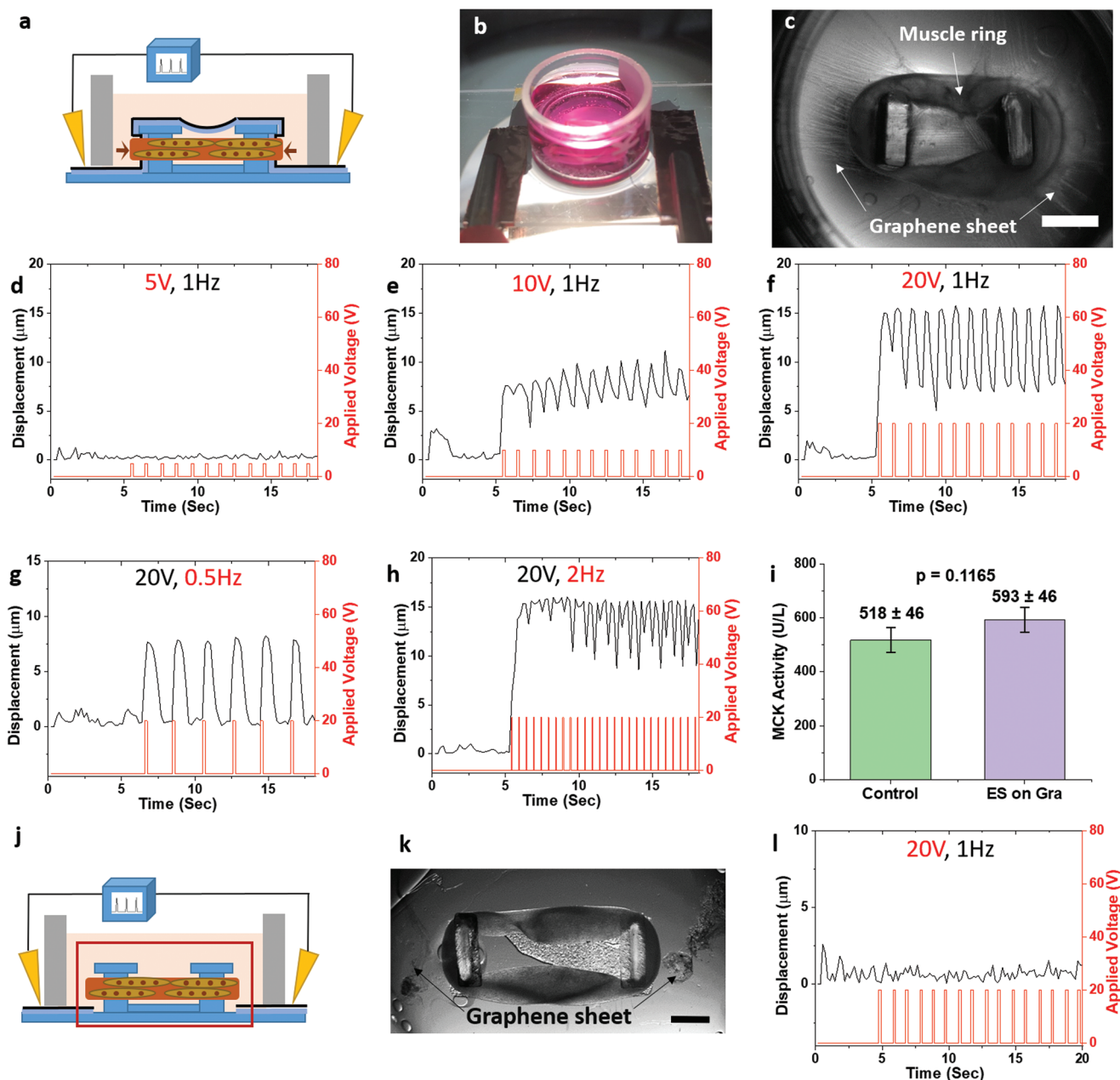


Figure 3. Electrical stimulation to the muscle ring through conformal graphene electrode. a) Schematic of the system and b) image of device for electrical stimulation. c) Optical image of the muscle ring on the graphene/PEG pillars. Scale bar is 2 mm. Displacement of pillars—time curves when graphene electrode was electrically stimulated by voltage amplitude of d) 5, e) 10, and f) 20 V, with 1 Hz and frequencies of g) 0.5 and h) 2 Hz at 20 V of voltage amplitude. i) Muscle creatine kinase (MCK) activities for muscle rings on pillars without graphene as a control group and graphene/PEG structure with electrical stimulation on the day 7 after differentiation ($n = 3$). Control experiment with graphene sheet only in contact with media separated from muscle ring. j) Schematic and k) optical image for electrical stimulation to muscle ring with graphene sheet not touching the muscle. l) No displacement of pillars is measured with time when graphene is not touching the muscle ring. Scale bar: 1 mm.

Figure 3h, a 2 Hz stimulation also matched with the movement from pillars, although the displacement did not fully recover to zero because of the viscoelastic properties of the printed PEGDA pillars. Figure S5 (Supporting Information) indicates that the amplitudes and frequencies of the pillar displacement caused by muscle twitching are proportional to the applied frequencies and voltages for electrical stimulation through the graphene electrode. Furthermore, muscle creatin kinase (MCK)

activity was measured for muscle ring with electrical stimulation through 3D graphene structure to observe the effect of electrical stimulation on muscle tissue, as shown in Figure 3i. Although muscle rings with electrical stimulation on 3D graphene appears to show slightly higher level of MCK activity than control group without graphene and electrical stimulation, the p value is 0.1165 considered to be not statistically significant. Our results show that the 3D transferred graphene electrode

can actuate the integrated muscle rings and availability of the platform for 3D muscle tissue model with electrical stimulation.

To confirm that the electric signals go through the graphene and not through the fluid medium, we designed another electrical stimulation experiment as shown in Figure 3j. Two pieces of graphene sheets were transferred to the glass substrate with the printed pillars such that they were not touching with pillars. The integrated muscle ring on the pillars did not contact the graphene sheets as shown in Figure 3k. When a 1 Hz, 20 V electrical pulse was applied to the graphene on the substrate, no change in pillar displacement was observed as shown in Figure 3l confirming that the electrical contacts do indeed function as they were designed to.

We report a biocompatible CVD graphene transfer method using a PEGDA supportive layer. The soft PEGDA layer enabled a 3D conformal integration of graphene with millimeter scaled 3D printed pillar and a muscle tissue ring. After the 3D transfer, Raman spectroscopy and electrical measurement results demonstrated a conductive graphene electrode on the 3D structure. The integrated muscle tissue ring also showed similar compaction during cell differentiation and subsequent cell viability as compared to control rings without the transferred graphene sheet. The integrated muscle ring responded to the electrical stimulation through the transferred graphene electrode with various applied voltages and frequencies. Our results demonstrate a new method for 3D graphene electrode integration as a potential platform for electrical applications for 3D biological tissue systems.

Supporting Information

Supporting Information is available from the Wiley Online Library or from the author.

Acknowledgements

This work was supported by National Science Foundation (NSF) Science and Technology Center Emergent Behavior of Integrated Cellular Systems (EBICS) (Grant No. CBET0939511), the Defense Threat Reduction Agency (DTRA) interagency Agreement No. 1620298, and partially by the NSF through the University of Illinois at Urbana-Champaign Materials Research Science and Engineering Center DMR-1720633. Research reported in this publication was also supported by the National Institutes of Health under Award No. T32EB019944. The content is solely the responsibility of the authors and does not necessarily represent the official views of National Institutes of Health.

Conflict of Interest

The authors declare no conflict of interest.

Keywords

3D graphene transfer, biohybrid robots, biological machines, PEGDA scaffolds, skeletal muscles

Received: August 19, 2019
Revised: December 16, 2019
Published online:

- [1] A. K. Geim, *Science* **2009**, *324*, 1530.
- [2] S. R. Shin, Y.-C. Li, H. L. Jang, P. Khoshakhlagh, M. Akbari, A. Nasajpour, Y. S. Zhang, A. Tamayol, A. Khademhosseini, *Adv. Drug Delivery Rev.* **2016**, *105*, 255.
- [3] M. T. Hwang, P. B. Landon, J. Lee, D. Choi, A. H. Mo, G. Glinsky, R. Lal, *Proc. Natl. Acad. Sci. USA* **2016**, *113*, 7088.
- [4] Kenry, W. C. Lee, K. P. Loh, C. T. Lim, *Biomaterials* **2018**, *155*, 236.
- [5] S. R. Shin, C. Zihlmann, M. Akbari, P. Assawes, L. Cheung, K. Zhang, V. Manoharan, Y. S. Zhang, M. Yuksekkaya, K.-T. Wan, M. Nikkahah, M. R. Dokmeci, X. Tang, A. Khademhosseini, *Small* **2016**, *12*, 3677.
- [6] P. Bajaj, J. A. Rivera, D. Marchwiani, V. Solovyeva, R. Bashir, *Adv. Healthcare Mater.* **2014**, *3*, 995.
- [7] S. J. Kim, K. W. Cho, H. R. Cho, L. Wang, S. Y. Park, S. E. Lee, T. Hyeon, N. Lu, S. H. Choi, D.-H. Kim, *Adv. Funct. Mater.* **2016**, *26*, 3207.
- [8] S. Ahadian, J. Ramon-Azcon, H. Chang, X. Liang, H. Kaji, H. Shiku, K. Nakajima, M. Ramalingam, H. Wu, T. Matsue, A. Khademhosseini, *RSC Adv.* **2014**, *4*, 9534.
- [9] E. Garcia-Tunon, S. Barg, J. Franco, R. Bell, S. Eslava, E. D'Elia, R. C. Maher, F. Guitian, E. Saiz, *Adv. Mater.* **2015**, *27*, 1688.
- [10] A. E. Jakus, E. B. Secor, A. L. Rutz, S. W. Jordan, M. C. Hersam, R. N. Shah, *ACS Nano* **2015**, *9*, 4636.
- [11] M. K. Shin, B. Lee, S. H. Kim, J. A. Lee, G. M. Spinks, S. Gambhir, G. G. Wallace, M. E. Kozlov, R. H. Baughman, S. J. Kim, *Nat. Commun.* **2012**, *3*, 650.
- [12] W. Li, J. Wang, J. Ren, X. Qu, *Adv. Mater.* **2013**, *25*, 6737.
- [13] X. Li, W. Cai, J. An, S. Kim, J. Nah, D. Yang, R. Piner, A. Velamakanni, I. Jung, E. Tutuc, S. K. Benerjee, L. Colombo, R. S. Ruoff, *Science* **2009**, *324*, 1312.
- [14] K. S. Kim, Y. Zhao, H. Jang, S. Y. Lee, J. M. Kim, K. S. Kim, J.-H. Ahn, P. Kim, J.-Y. Choi, B. H. Hong, *Nature* **2009**, *457*, 706.
- [15] M. Lanza, A. Bayerl, T. Gao, M. Porti, M. Nafria, G. Y. Jing, Y. F. Zhang, *Adv. Mater.* **2013**, *25*, 1440.
- [16] W. Shim, K. A. Brown, X. Zhou, B. Rasin, X. Liao, C. A. Mirkin, *Proc. Natl. Acad. Sci. USA* **2012**, *109*, 18312.
- [17] J. Choi, H. J. Kim, M. C. Wang, J. Leem, W. P. King, S.W. Nam, *Nano Lett.* **2015**, *15*, 4525.
- [18] J. L. P. Morin, N. Dubey, F. E. D. Decroix, E. K. Luong-Van, A. H. Castro Neto, V. Rosa, *2D Mater.* **2017**, *4*, 025060.
- [19] R. M. Duffy, A. W. Feinberg, *Wiley Interdiscip. Rev.: Nanomed. Nanobiotechnol.* **2014**, *6*, 178.
- [20] L. Riccoti, B. Trimmer, A. W. Feinberg, R. Raman, K. K. Parker, R. Bashir, M. Sitti, S. Martel, P. Dario, A. Menciassi, *Sci. Rob.* **2017**, *2*, eaaq0495.
- [21] M. S. Sakar, D. Neal, T. Boudou, M. A. Borochin, Y. Li, R. Weiss, R. D. Kamm, C. S. Chen, H. H. Asada, *Lab Chip* **2012**, *12*, 4976.
- [22] R. Raman, C. Cvetkovic, R. Bashir, *Nat. Protoc.* **2017**, *12*, 519.
- [23] G. J. Pagan-Diaz, X. Zhang, L. Grant, Y. Kim, O. Aydin, C. Cvetkovic, E. Ko, E. Solomon, J. Harris, H. Kong, T. Saif, R. Bashir, *Adv. Funct. Mater.* **2018**, *28*, 1801145.
- [24] Z. Li, Y. Seo, O. Aydin, M. Elhebeary, R. D. Kamm, H. Kong, M. T. A. Saif, *Proc. Natl. Acad. Sci. USA* **2019**, *116*, 1543.
- [25] Y. Jin, M. Sun, D. Mu, X. Ren, Q. Wang, L. Wen, *Electrochim. Acta* **2012**, *78*, 459.
- [26] D. Yamini, G. D. Venkatasubbu, J. Kumar, V. Ramakrishnan, *Spectrochim. Acta, Part A* **2014**, *117*, 299.
- [27] S.-A. Peng, Z. Jin, P. Ma, D.-Y. Zhang, J.-Y. Shi, J.-B. Niu, X.-Y. Wang, S.-Q. Wang, M. Li, X.-Y. Liu, T.-C. Ye, Y.-H. Zhang, Z.-Y. Chen, G.-H. Yu, *Carbon* **2015**, *82*, 500.
- [28] G. Jo, M. Choe, S. Lee, W. Park, Y. H. Kahng, T. Lee, *Nanotechnology* **2012**, *2*, 11201.